Axion cooling of neutron stars. II. Beyond hadronic axions

Armen Sedrakian

Frankfurt Institute for Advanced Studies, Ruth-Moufang str. 1, D-60438 Frankfurt-Main, Germany

(Received 4 October 2018; published 25 February 2019)

We study the axion cooling of neutron stars within the Dine-Fischler-Srednicki-Zhitnitsky (DFSZ) model, which allows for tree-level coupling of electrons to the axion and locks the Peccei-Quinn charges of fermions via an angle parameter. This extends our previous study [Phys. Rev. D **93**, 065044 (2016)] limited to hadronic models of axions. We explore the two-dimensional space of axion parameters within the DFSZ model by comparing the theoretical cooling models with the surface temperatures of a few stars with measured surface temperatures. It is found that axions masses $m_a \geq 0.06$ to 0.12 eV can be excluded by x-ray observations of thermal emission of neutron stars (in particular by those of Cas A), the precise limiting value depending on the angle parameter of the DFSZ model. It is also found that axion emission by electron bremsstrahlung in neutron star crusts is negligible except for the special case where neutron Peccei-Quinn charge is small enough, so that the coupling of neutrons to axions can be neglected.

DOI: 10.1103/PhysRevD.99.043011

I. INTRODUCTION

Axions were suggested four decades ago [1,2] to solve the strong-CP problem in QCD [3]. They are one of the viable candidates for the cold dark matter in cosmology and can play an important role in the stellar astrophysics. Axions are identified with the pseudo-Goldstone bosons which emerge through the spontaneous breaking of the approximate Peccei-Quinn (PQ) global $U(1)_{PQ}$ symmetry [4,5]. Their coupling to the Standard Model (SM) particles is determined by a decay constant f_a and PQ charges of the SM particles. For reviews of searches of axions in experiments and limits on their properties from astrophysics see Refs. [6–8].

In a previous work [9] (hereafter Paper I) the axion cooling of neutron stars was studied on the basis of numerical simulations, with the aim of placing constraints on the axion coupling (or, equivalently, the mass m_a) through comparison of the simulation results for neutron star surface temperatures with the observed surface photon luminosities of a few well-studied objects. As in the case of the Sun, solar-type stars, red giant stars, white dwarfs, and supernovae constraints on axion properties can be obtained by requiring that the coupling of axions to SM particles should not alter significantly the agreement between theoretical models and observations [10,11]. In Paper I the PQ charges of constituents of neutron star matter were chosen according to the *hadronic model* of axions, i.e., the Kim-Shifman-Vainstein-Zakharov (KSVZ) model [12,13]. In this model protons and neutrons have nonzero PQ charges and, therefore, couple to the axion at the tree level. On the contrary, electron's PQ charge is zero, i.e., the axion does not couple to the electron at the tree level. In an alternative Dine-Fischler-Srednicki-Zhitnitsky (DFSZ) axion model [14,15] electrons have nonzero PQ charges, therefore the electronic component of a neutron star can cool by emitting axions. Furthermore, in the DFSZ model the couplings of the SM particles depend only on an angle parameter and f_a, which limits the parameter space of this model to a two-dimensional plane. It is the purpose of this work to adapt and extend the computations reported in Paper I to the DFSZ axion model. A new aspect of this study is the additional axion emission through the electronic component of the star, which contributes alongside the axion emission by hadrons studied in detail in Paper I. Another novelty is the "locking" of the fermionic PQ charges via an angle parameter in the DFSZ model, which restricts the parameter space and, therefore, facilitates the parameter study of cooling curves.

A number of complementary studies of axion cooling of neutron stars have recently used the data on compact central objects (CCOs) to place limits on the axion properties. The transient behavior of the Cas A has been studied in Refs. [16,17] to this end and useful limits were obtained assuming that the data reflect *per se* the fast cooling of this object. The cooling behavior of peculiarly "hot" CCO HESS J1731-347 has been analyzed in the context of axionic cooling in Ref. [18].

This paper is structured as follows: In Sec. II we start with a brief review of axion emission processes, discuss the axion coupling to SM particles within the DFSZ model and concentrate on the rate of axion emission by electron bremsstrahlung in neutron star crusts. Sec. III discusses the simulation setup and the resulting cooling tracks for a large array of models of neutron stars. Our conclusions and an outlook are given in Sec. IV. The natural units with

$\hbar = c = k_B = 1$, $\alpha = 1/137$ will be used unless stated otherwise.

II. MICROPHYSICS OF AXION EMISSION IN NEUTRON STARS

A. Overview

The focus of this work, from the microscopic point of view, is the bremsstrahlung of axions by electrons which are scattered on nuclei in neutron star crusts. This process has been initially studied in Ref. [19]. Improved rates which include many-body correlations were derived later in Refs. [20,21]. However, these rates have not been implemented in cooling simulations of neutron stars previously; the pioneering simulations of Umeda *et al.* [22] contain results obtained within the DFSZ model, but the electron bremsstrahlung process has not been mentioned. As indicated above, our simulations in Paper I were limited to hadronic KSVZ model which does not couple the axions to electrons at the tree level. Nevertheless, the electron bremsstrahlung of axions was considered in detail in the context of cooling of white dwarfs [23–26] and appropriate limits on the electron-axion coupling were derived from comparisons of white-dwarf cooling models and their observations. We will discuss the implementation of this process in the following subsection.

A leading axion emission process from the interiors of neutron stars is the axion (a) bremsstrahlung by nucleons (N): $N + N \to N + N + a$. It was studied in the context of type-II supernovae and the bounds on axion properties were derived by requiring consistency between the explosion energetics as well as energies of neutrinos observed in the 1987A event and energy drained by axion emission [27–31]. More recent work concluded that future supernova observations could probe axion mass range $m_a \leq 10^{-2}$ eV [32]. Axions may not free stream in supernovae if their coupling to matter is large enough. Reference [29] finds that axions are trapped within a newborn neutron star if the axion mass is larger than 10^{-2} eV. This implies the existence of an "axion sphere," i.e., a surface of last interaction of axions with the ambient matter at the initial stage of neutron star evolution. However the physics at the early moments of neutron star cooling does not affect the following stages of thermal evolution significantly, therefore our simulations are started at a temperature at which axions and neutrinos are untrapped, which is typically $T \simeq 5$ MeV.

Axion bremsstrahlung via Cooper pair-breaking-formation (PBF) processes sets in after the nucleons undergo a superfluid phase transition [9,33]. These have been the dominant axion emission processes in the KSVZ model. Our previous limits reflect the efficacy of these processes in cooling neutron stars below the observed temperatures in the *neutrino cooling era*, which corresponds to the time span $0.1 \leq t \leq 100$ kyr. It is understood that their neutrino counterpart PBF processes [34–38] are sufficient to cool the stars towards their current observational values. Interestingly, PBF processes can trap axions at the late stages of cooling if $f_a \leq 10^6$ GeV due to the inverse proton PBF, as has been pointed out in Ref. [17]. The f_a-values discussed below are all above this limit, therefore we will ignore the possibility of axions being trapped.

B. DFSZ model of axion coupling to SM particles

The Lagrangian of axion field a has the form

$$\mathcal{L}_a = -\frac{1}{2}\partial_\mu a \partial^\mu a + \mathcal{L}^{(N)}_{\rm int}(\partial_\mu a, \psi_N) + \mathcal{L}^{(L)}_{\rm int}(a, \psi_L), \qquad (1)$$

where the second and third terms describe the coupling of the axion to the nucleonic (ψ_N) and leptonic fields (ψ_L) of the SM. The second term is given explicitly by the interaction Lagrangian

$$\mathcal{L}^{(N)}_{\rm int} = \frac{1}{f_a} N^\mu \partial_\mu a, \qquad N^\mu = \sum_N \frac{C_N}{2}\bar{\psi}_N \gamma^\mu \gamma_5 \psi_N, \qquad (2)$$

where $N \in n$, p stands for neutron or proton, N^μ is the baryon current, f_a is the axion decay constant, and C_N is the PQ charge of baryon N. The coupling of axions to electrons can be written in the pseudoscalar form

$$\mathcal{L}^{(e)}_{\rm int}(a, \psi_e) = \frac{C_e}{2f_a}\bar{\psi}_e \gamma^\mu \gamma_5 \psi_e (\partial_\mu a) = -i g_{ae} \bar{\psi}_e \gamma_5 \psi_e a, \qquad (3)$$

where the Yukawa coupling is given by $g_{ae} = C_e m_e / f_a$ with m_e being the electron mass. We will also use a "fine-structure constant" associated with this coupling, which is defined as $\alpha_{ae} = g^2_{ae}/4\pi$.

The PQ charges for the proton and neutron are given by generalized Goldberger-Treiman relations

$$C_p = (C_u - \eta)\Delta_u + (C_d - \eta z)\Delta_d + (C_s - \eta w)\Delta_s, \qquad (4)$$

$$C_n = (C_u - \eta)\Delta_d + (C_d - \eta z)\Delta_u + (C_s - \eta w)\Delta_s, \qquad (5)$$

where $\eta = (1 + z + w)^{-1}$, with $z = m_u/m_d$, $w = m_u/m_s$, $\Delta_u = 0.84 \pm 0.02$, $\Delta_d = -0.43 \pm 0.02$ and $\Delta_s = -0.09 \pm 0.02$. The main uncertainty arises from the quark-mass ratios: $0.35 \leq z \leq 0.6$ and $17 \leq m_s/m_d \leq 22$. We adopt below the following mean values: $z = 0.5$ and $w = 0.025$.

In the DFSZ model, the PQ charges are given by

$$C_e = C_d = C_s = \frac{\cos^2\beta}{3}, \qquad C_u = \frac{\sin^2\beta}{3}, \qquad (6)$$

where the angle β is a free parameter.

TABLE I. The values of the axion-nucleon and axion-electron coupling constants for various values of parameter $\cos^2\beta$.

$\cos^2\beta$	C_n	C_p	C_e
0.0	−0.14	−0.13	0.00
0.25	−0.04	−0.24	0.08
0.5	0.06	−0.36	0.17
0.75	0.16	−0.47	0.25
1.0	0.26	−0.58	0.33

Finally, the axion mass is given by

$$m_a = \frac{z^{1/2}}{1+z}\frac{f_\pi m_\pi}{f_a} = \frac{0.6\ \text{eV}}{f_{a7}}, \tag{7}$$

where $f_{a7} = f_a/(10^7\ \text{GeV})$, the pion mass $m_\pi = 135$ MeV, its decay constant is $f_\pi = 92$ MeV, and $z = 0.5$ as above. Note that Eq. (7) translates a lower bound on f_a into an upper bound on the axion mass. Table I displays the set of axion-fermion couplings for five values of the parameter $\cos^2\beta$ which are used below to cover the relevant range of cooling simulations. In addition, we show in Fig. 1 the same dependence in the full range $0 \le \cos^2\beta \le 1$.

C. Axion bremsstrahlung emission in the crust

At temperatures relevant for *neutrino cooling era* the dominant cooling process associated with the electron component of the star is the electron bremsstrahlung of neutrino–anti-neutrino pairs or axions when electrons are scattered off the nuclei. For all relevant temperatures and densities, ions are fully ionized and electrons form an ultrarelativistic, weakly interacting gas. The correlations in the ionic component are characterized by the Coulomb plasma parameter

$$\Gamma = \frac{e^2Z^2}{Ta_i} \simeq 22.73\frac{Z^2}{T_6}\left(\frac{\rho_6}{A}\right)^{1/3}, \tag{8}$$

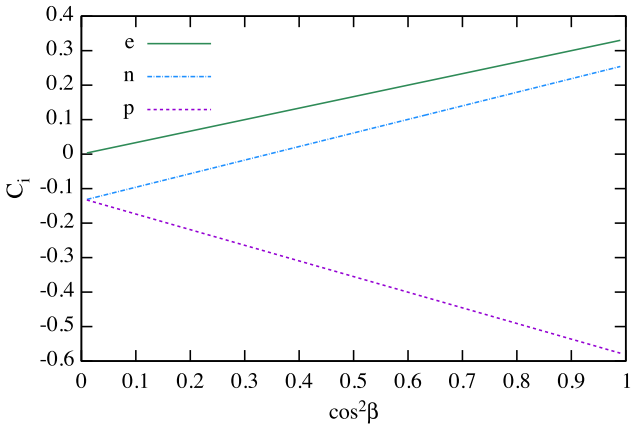

FIG. 1. Dependence of the PQ charges of the electron (e), neutron (n) and proton (p) on the parameter $\cos^2\beta$.

where e is the elementary charge, A and Z are the mass number and charge of a nucleus, T is the temperature, $a_i = (4\pi n_i/3)^{-1/3}$ is the radius of the spherical volume per ion, n_i the number density of nuclei, T_6 is the temperature in units 10^6 K, and ρ_6 is the density in units of 10^6 g cm^{-3}. The ionic component is in the liquid state for values of $\Gamma \le \Gamma_m \simeq 180$. Otherwise, it forms a lattice, i.e., for $\Gamma > \Gamma_m$ the electrons are scattering on the lattice and phonons. For a recent compilation of the phase diagram of matter in the crust of a neutron star and its dependence on the composition of matter see Ref. [39].

The axion emissivity can be written in the solid (S) and liquid (L) phases in the generic form [19–21]

$$\epsilon_{L/S} = \frac{4\pi^2}{15}\frac{(\alpha Z)^2}{A}\frac{\alpha_{ae}n_B}{\hbar^2 c}\frac{(k_BT)^4}{(2cp_F)^2}\left(\frac{p_F}{m_e}\right)^2 F_{L/S}, \tag{9}$$

where for the sake of clarity we recovered the fundamental constants, p_F is the Fermi momentum of electrons, $n_B = An_i$ is the nucleon number density, and $F_{L/S}$ are correlation functions defined in Refs. [20,21]. They depend (among other factors) on the static structure factor of ions and the nuclear form-factor of the nucleus. After substituting the numerical constants one finds [20,21]

$$\epsilon_{L/S} = 1.08\rho\alpha_{ae,26}\frac{Z^2}{A}T_8^4F_{L/S}\ [\text{erg cm}^{-3}\,\text{s}^{-1}], \tag{10}$$

where ρ is the mass density, $T_8 = T/(10^8K)$ and $\alpha_{ae26} = 10^{26}\alpha_{ae}$ with $g_{ae} = \sqrt{4\pi\alpha_{ae}} = C_em_e/f_a \simeq 1.67\times 10^{-11}\cos^2\beta/f_{a7}$. The correlation functions in the solid and liquid phases were obtained through fits to the data provided in Fig. 3 of Ref. [20]. In the solid phase the contribution of the lattice is taken into account, but the small phonon contribution is neglected, see Fig. 3 of Ref. [21]. For practical purposes, we use fits to these computations which are given in the Appendix.

III. COOLING SIMULATIONS

To make our presentation self-contained we remind here the basic assumptions underlying the strategy adopted in Paper I: (a) the simulations are based on a conservative model of cooling of neutron stars, which requires that the stellar models describing the data are not massive enough to allow for fast cooling processes to occur. This requirement is based on the observation that fast cooling agents appear only above certain density threshold which can be reached only in massive compact stars. The light- to medium-mass neutron stars within the mass range $1 \le M/M_\odot \le 1.8$ are good candidates for such cooling. (b) The simulations are compared to observational data for sources with estimated magnetic fields of the order of canonical pulsar fields $B \simeq 10^{12}$ G and below. This ensures that internal heating by strong magnetic fields [40] can be excluded. (c) We

continue to use the NSCool code[1] with its specific microphysics input to guarantee the easy reproduction of our results and to benchmark the axion cooling of neutron stars (see Paper I for details). The code has been extended to include all the relevant axionic emission processes by hadrons and electrons as discussed above.

A. Physics input and observational data

The cooling code solves the energy balance and transport equations in spherical symmetry, i.e., rotation and magnetic fields are excluded. We use a generic relationship between the surface temperature T_s and the temperature of the shell at density $\rho_b = 10^{10}$ g cm^{-3} to avoid the problem of radiative transport in the thin blanket lying below this density. This relation is given by $T_s^4 = g_s h(T)$, where g_s is the surface gravity, and h is some function which depends on the temperature T, the opacity of the blanket, and its equation of state. The surface composition of a neutron star is modeled by the parameter η, with $\eta = 0$ corresponding to a purely iron surface and $\eta \to 1$ to a light-element surface. Further details of the input physics can be found in Ref. [41] and in Paper I. Throughout a cooling simulation, we extract the neutrino and axion luminosities of our models, as well as the photon luminosity which is given by the Stefan-Boltzmann law $L_\gamma = 4\pi\sigma R^2 T_s^4$, where σ is the Stefan-Boltzmann constant, and R is the radius of the star.

The dataset of surface temperatures considered in Paper I, which we also use here is as follows. The first object—the *CXO J232327.9+584842* in the Cassiopeia A (Cas A) supernova remnant (SNR)—is a representative of a group of central compact objects (CCOs)—pointlike, thermally emitting x-ray sources located close to the geometrical centers of nonplerionic SNRs [42]. These objects have low magnetic fields, which exclude heating processes at this stage of evolution. The value $T = 2.0 \pm 0.18 \times 10^6$ K at the age 320 yr was used [43]. In addition three nearby neutron stars which allow spectral fits to their x-ray emission were considered [44]. The fits invoke two black-body temperatures and we identify the lowest one with the surface temperature and quote only this value (see for further details Paper I):

(i) *PSR B0656+14* with fit temperatures $T_w = (6.5 \pm 0.1) \times 10^5$ K and characteristic age 1.1×10^2 kyr.
(ii) *PSR B1055-52* with fit temperatures $T_w = 7.9 \pm 0.3 \times 10^5$ K and characteristic age 5.37×10^2 kyr.
(iii) *Geminga*, a radio-quiet object, with the $T_w = 5.0 \pm 0.1 \times 10^5$ K and characteristic age 3.4×10^2 kyr.

The error in the estimate of the ages of these objects from their spin-down age is quantified by varying their age by a factor of 3. As noted in Paper I, the data on PSR B1055-52 are marginally consistent with the cooling curves even in the absence of axions. This can be attributed to (a) larger error in the age of this pulsar than assumed above; (b) internal heating; (c) the modeling of the pairing gaps, which in principle can be tuned to fit the inferred temperature of PSR B1055-52. Given the uncertainties involved, we will exclude the data on PSR B1055-52 in the following. We do not attempt to fit the transient behavior of the Cas A, as has been done in Refs. [16,17], since the data on rapid cooling is inconclusive [43,45]. In any case, the limits derived by these authors using cooling simulations are comparable to those derived below. Future observations and analysis of putative fast cooling of Cas A may prove to be a highly efficient tool to constrain the properties of axions along the lines of Refs. [16,17]. An additional candidate for constraining axion properties is the peculiarly "hot" CCO HESS J1731-347. Reference [18] derived already limits on f_{a7} from cooling simulations using the data from this object. Since this object challenges our understanding of the cooling of neutron stars even without axionic cooling we will not include it in our data set; see Ref. [18] for an alternative.

B. Results of simulations

A representative collection of 20 models of cooling neutron stars for four values of the axion decay constant $f_{a7} = 20, 15, 10, 5$ and the PQ changes specified by rows 1 to 5 in Table I were simulated. The mass of each model was kept fixed at 1.4 $M_\odot$ assuming the "APR-Cat" equation of state of the NSCool code. The triple of neutron $^1S_0$ and $^3P_2$-$^3F_2$ and proton $^1S_0$ gaps were fixed to the value "WAP-b-T73" of the NSCool code, where the acronyms refer to Ref. [46] (WAP), model b of Ref. [47] (b), and Ref. [48] (T73). We note that WAP and T73 gap values can be considered as lower bounds on the neutron and proton $^1S_0$ gaps respectively. Model b of Ref. [47] can be taken as an upper limit on the $^3P_2$-$^3F_2$ gap; we shall consider alternatives below.

Figures 2 and 3 show the results of cooling simulations of 20 models of $m = M/M_\odot = 1.4$ mass neutron stars defined above with a nonaccreted iron envelope ($\eta = 0$) and a light-element envelope ($\eta = 1$), respectively. Each of the panels corresponds to a value of the axion coupling $f_{a7} = 20$, 15, 10 and 5; within each panel, we vary the PQ charges of neutrons, protons and electrons according to the indicated values of $\cos^2\beta$ parameter. The dots with error bars show the three test objects quoted above. Quite generally, the temperature of CCO in Cas A is consistent with the cooling curves if one assumes a light-element envelope in the absence of axion cooling; otherwise, its theoretical temperature undershoots the observational value. In the case of older pulsars, the data agrees with the predictions of the theoretical modeling without axion cooling only for an iron envelope.

Consider now switching on the axion production in the case $\eta = 0$ shown Fig. 2. The additional loss of energy by axion emission decreases the temperatures of our models.

[1]The NSCool code is available at: http://www.astroscu.unam.mx/neutrones/NSCool/.

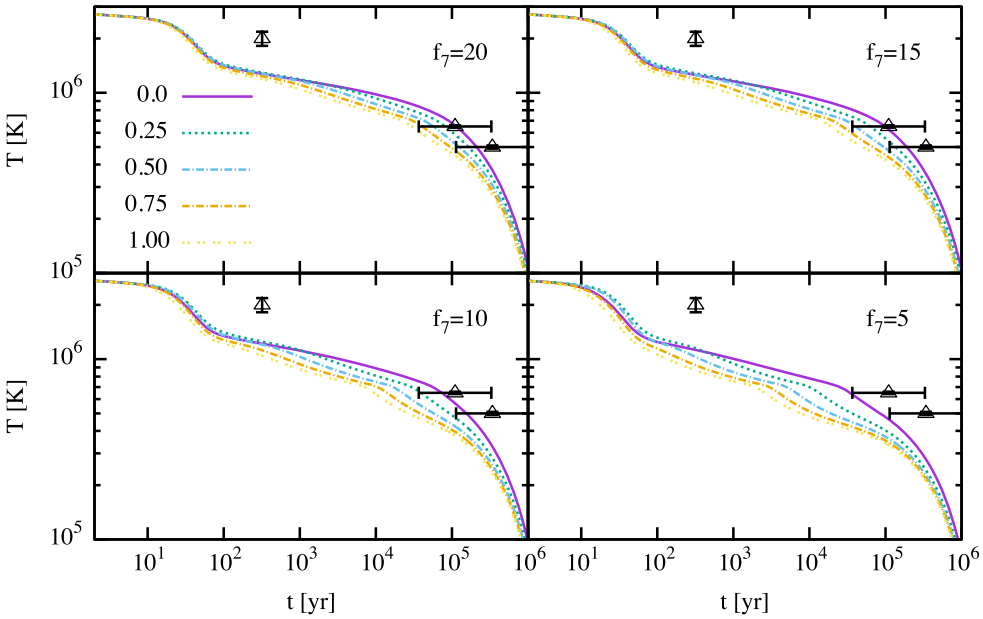

FIG. 2. Cooling tracks of neutron star models with mass $M = 1.4\ M_\odot$ for the case of a nonaccreted iron envelope ($\eta = 0$). The data shows the surface temperatures inferred from the black-body fits to the x-ray emission of CCO in Cas A, PSR B0656 + 14 and Geminga. Each panel corresponds to fixed value of f_{a7} as indicated. The values of PQ charges are specified in terms of $\cos^2\beta$ parameter, see Table I.

For $f_{a7} = 20$ all the five values of PQ charges are consistent with the data; for $f_{a7} = 15$ the values $\cos^2\beta = 0.75$ and larger are excluded by the data; for $f_{a7} = 10$ the values larger than $\cos^2\beta = 0.5$ are incompatible with the data; finally, for $f_{a7} = 5$ all values of $\cos^2\beta$ are excluded by the data, except for $\cos^2\beta = 0$.

Similar, but not identical, conclusions are reached by examining the data in Fig. 3. One observes that the following combinations are inconsistent with the Cas A data: $f_{a7} = 10$ and $\cos^2\beta = 1.0$ and $f_{a7} = 5$ and $\cos^2\beta \geq 0.25$. None of the values of the PQ charges are excluded for $f_{a7} = 15$ and 20.

Figures 4 and 5 show the neutrino, axion and photon luminosities as a function of time for four values of the axion coupling constant f_{a7} and PQ charges corresponding to $\cos^2\beta = 0.5$ and $\cos^2\beta = 1$ (see Table I) in the cases $\eta = 0$ and $\eta = 1$, respectively. Clearly, the figures differ only by the values of the surface photon luminosity, which

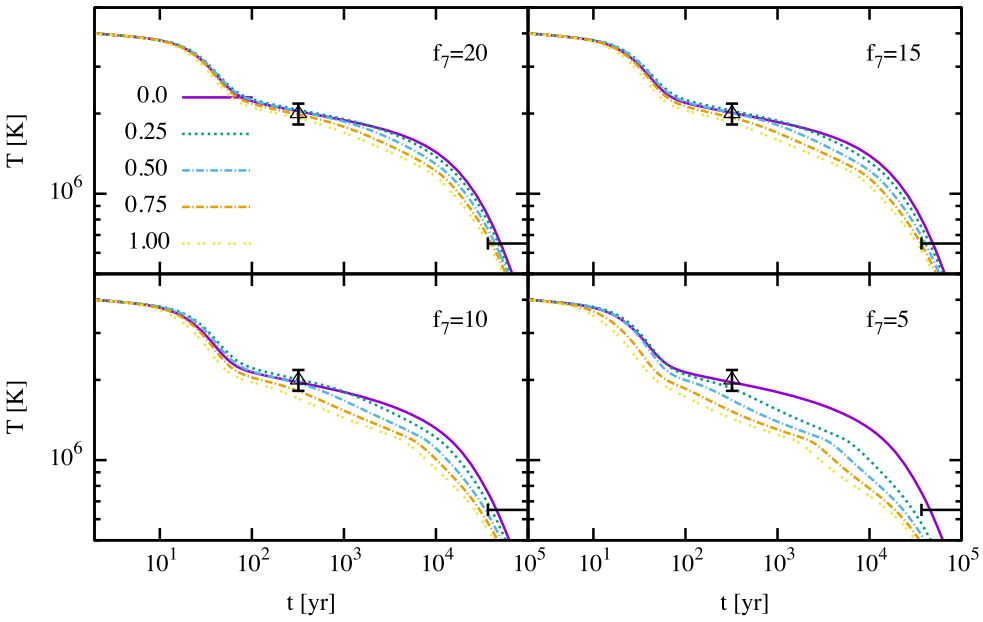

FIG. 3. Same as in Fig. 2 but for $\eta = 1$.

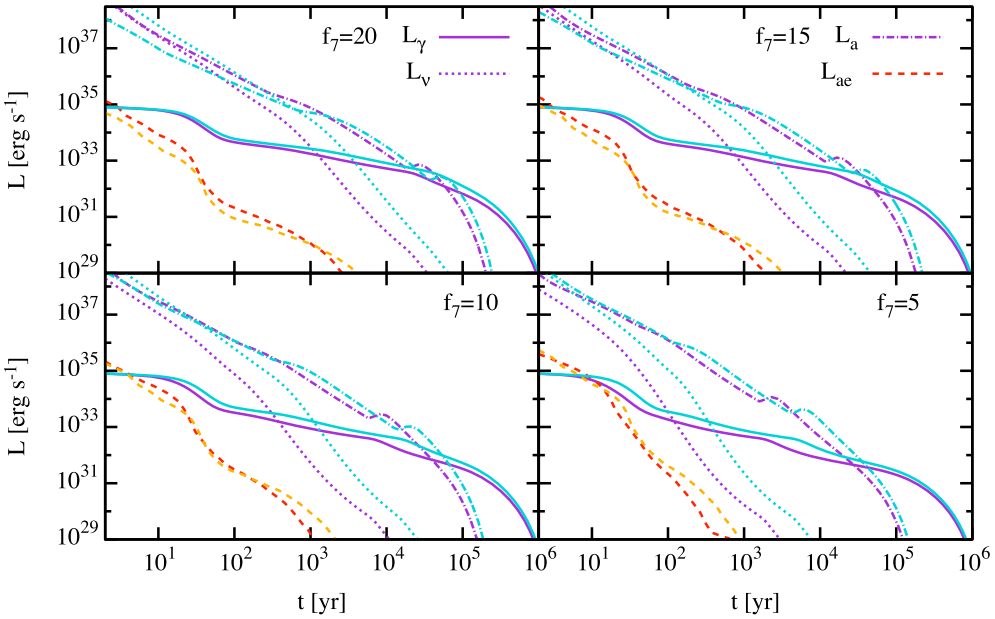

FIG. 4. Dependence of the photon L_γ, neutrino L_ν and axion L_a luminosities on age for the models of $M = 1.4\ M_\odot$ stars for indicated values of the axion coupling f_{a7}. The PQ charges correspond to $\cos^2\beta = 0.5$ (light blue) and $\cos^2\beta = 1$ (violet). In addition we show the axion luminosity L_{ae} due to electron bremsstrahlung in the crust [with emissivity given by Eq. (10)] for $\cos^2\beta = 0.5$ (red) and $\cos^2\beta = 1$ (orange).

is larger in the case $\eta = 1$ at early stages of thermal evolution and the opposite is true at later stages of evolution. It is seen that for $f_{a7} = 20$ the axion and neutrino luminosities are comparable. In the remaining cases, the neutrino luminosity is subdominant and the cooling rate is determined by the balance between the axion emission rate and the change in the thermal energy given approximately by $c_V dT/dt$, where c_V is the net specific heat of the star.

To quantify the role of the electron bremsstrahlung of axions in the crust of a neutron star we show its luminosity L_{ae} in Fig. 4. Irrespective of the value of f_{a7} its contribution to axionic luminosity is negligibly small for $\cos^2\beta = 0.5$ and 1; while its magnitude is comparable to the photon

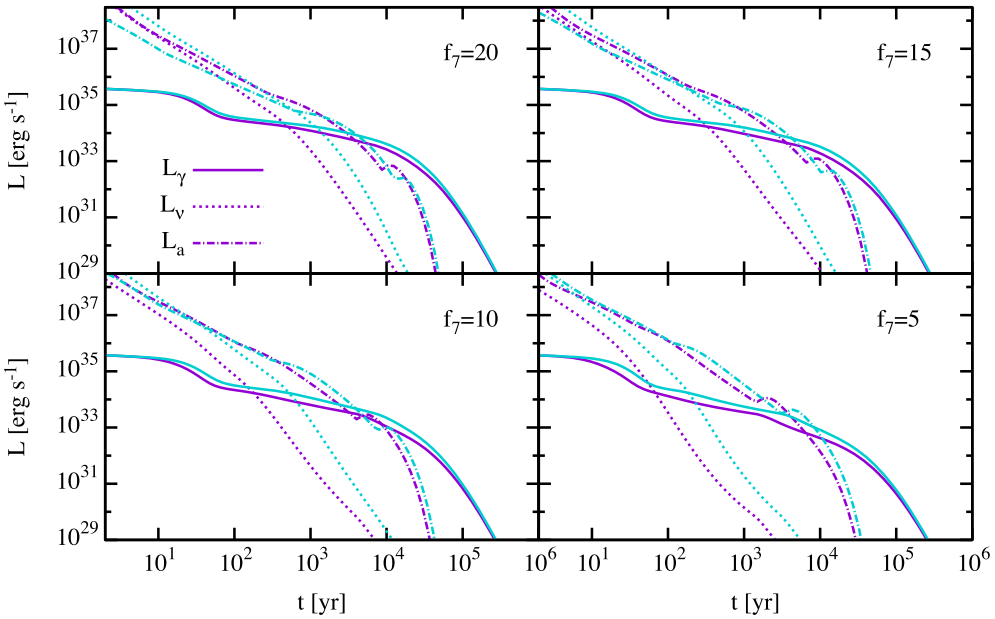

FIG. 5. Same as in Fig. 4 but for $\eta = 1$, in which case the photon luminosity is modified, but the neutrino and axion luminosities are not.

luminosity and even exceeds it for $f_{a7} \sim 5$, this occurs only at the early stages of evolution where the axion and neutrino emission by other processes dominate. However, the bremsstrahlung may contribute to the axion luminosity in some regions of the parameter space. Consider the case where the axion-neutron coupling $C_n = 0$, which corresponds to $\cos^2\beta = 0.344$, see Fig. 1. In this case, the PBF processes on neutron condensates in the core and the crust do not contribute to axion emission. Then, the net axion luminosity is determined by the electron bremsstrahlung, the PBF process in the proton condensate, and proton modified Urca process. To disentangle the last two processes we consider two cases: (a) the proton gap vanishes in which case the proton PBF process vanishes as well; (b) the proton gap is finite and is given by T73 [48]. In case (a) the axionic cooling is the sum of the electron bremsstrahlung and modified Urca process. Figure 6 shows that up to $\sim 10^2$ yr the electron bremsstrahlung can contribute a substantial fraction to the net axion luminosity in both cases (a) and (b). Of course, we consider only very special case of $C_n = 0$; as seen in Fig. 4 once neutrons couple to axions their axion emissivity completely dominates the electron bremsstrahlung. Note that the magnitude of the axion luminosity as measured with respect to the neutrino luminosity changes with the value f_{a7}, whereas the relative magnitude of the luminosities of various axionic processes do not. This is a straightforward consequence of the f_a^{-2} scaling of the rates given by tree-level amplitudes.

The modeling of neutron star cooling depends on a large number of parameters in general, but it is known to be most sensitive to the pairing gaps of neutrons and protons. To gain some insight in the effect of variation of these gaps, cooling simulations were performed with alternate pairing gaps for each type of the condensate while leaving the others fixed at their assumed values given by the triple WAP-b-T73 defined above and taken as a reference for comparison. Figure 7 shows the pairing gaps or critical temperatures for neutron $^1S_0$ and $^3P_2$-$^3F_2$ pairing and proton $^1S_0$ pairing. The reference gap in the neutron star crusts represents a lower limit (as it includes the suppression by long-range polarization effects). As an alternative we use the computation of Ref. [49] where the pairing

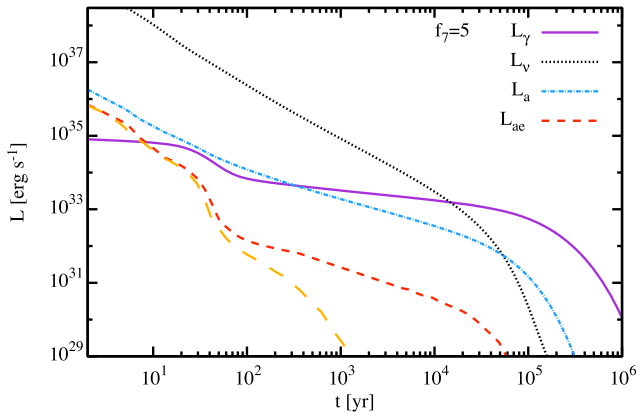

FIG. 6. Axion and neutrino luminosities of a neutron star model with mass $M = 1.4\,M_\odot$ for the case of a nonaccreted iron envelope ($\eta = 0$) and $f_{a7} = 2$. We consider the value $\cos^2\beta = 0.344$ in which case $C_p = -0.284$, $C_e = 0.115$ and $C_n = 0$ (neutrons do not couple to the axions). The luminosity of axion bremsstrahlung by electrons L_{ae} is shown for proton $^1S_0$ gap $\Delta_p = 0$ (short dashed) and for gap values from Ref. [48] (long dashed).

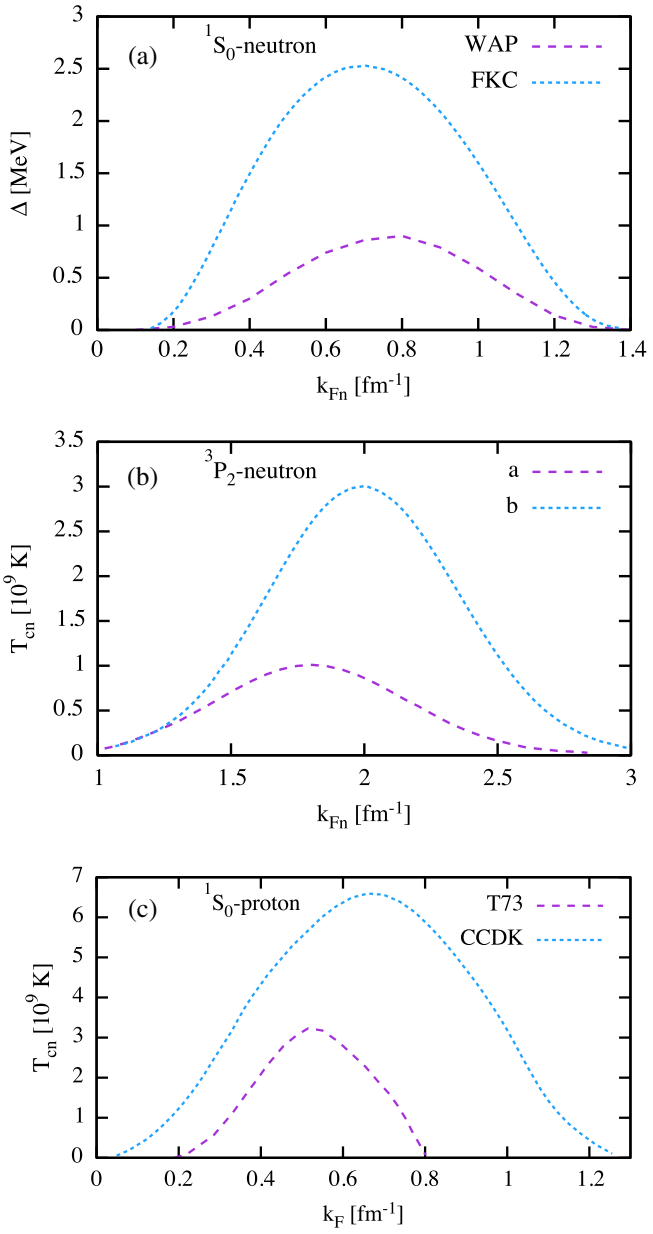

FIG. 7. Pairing gaps (critical temperatures) used in the simulations in Fig. 8 as a function of neutron (proton) Fermi momentum. (a) neutron $^1S_0$-gaps according to WAP [46] and FCK [49]; (b) critical temperature of $^3P_2$-$^3F_2$ superfluid neutron phase transition according to models a and b of Ref. [47]; (c) critical temperature of $^1S_0$ superfluid proton phase transition according to T73 [48] and CCDK [50].

interaction resums both long- and short-range correlation in an approximated way. The resulting gap is significantly larger, the maxima differing by a factor ∼2.5. The reference value of the critical temperature for neutron $^3P_2$-$^3F_2$ pairing is large and we need to adopt a smaller value; we consider below two options where $T_c = 0$ in this channel or it is given by the model a (instead of b) of Ref. [47]. Finally, for proton $^1S_0$ pairing we explore the possibility of larger T_c, taking as an example the one corresponding to the gap given by Ref. [50]. The corresponding critical temperature has a maximum by a factor of 2 larger and a substantially larger extent into the core of the star.

We start with the case of vanishing neutron $^3P_2$-$^3F_2$ gap [panel (a) of Fig. 8]. This results in moderately enhanced temperatures, the uncertainty being of the order of 5% except during the late time cooling $t > 10^5$ yr where significant differences arise. Adopting a smaller value of the $^3P_2$-$^3F_2$ gap [panel (b)] we find that cooling tracks drop earlier to lower temperatures at $t \sim 10^2$ yr and the temperatures stay lower throughout the neutrino-axion cooling era $t \leq 10^5$ yr. This implies that lower values of the pairing $^3P_2$-$^3F_2$ gap cannot affect the limits inferred using its reference value. Employing a larger neutron $^1S_0$ pairing gap [49] in the crusts [panel (c)] leads to an earlier drop in the cooling curves at 10^2 yr and temperatures beyond this timescale almost identical to the reference ones; this in turn implies that the inferred limits will not be affected with the variations of the neutron $^1S_0$ gap. Finally, if one adopts a larger proton $^1S_0$ gap [50] (panel d) the drop in the cooling curves is larger at $t \leq 10^2$ yr. In this case the deviations are again not large, of the order of 10% for $t \leq 10^5$ yr. We conclude that the variations in the values of the gaps in neutron and proton condensates do not affect significantly the limits drawn from the analysis of the cooling curves.

In the case of Cas A the age of the CCO is known, therefore its average temperature provides a reliable reference value. In the parameter space spanned by $\cos\beta^2$ and f_7 we can now deduces the limiting values of these parameters. As seen from Fig. 3, in the range $0 \leq \cos\beta^2 \leq 1$ the compatibility with the data implies $5 \leq f_{a7} \leq 10$. Using Eq. (7) we find upper limits on axion masses

$$\max[m_a] \simeq 0.12 \text{ eV}, \qquad \cos^2\beta \simeq 0, \tag{11}$$

$$\max[m_a] \simeq 0.06 \text{ eV}, \qquad \cos^2\beta \simeq 1. \tag{12}$$

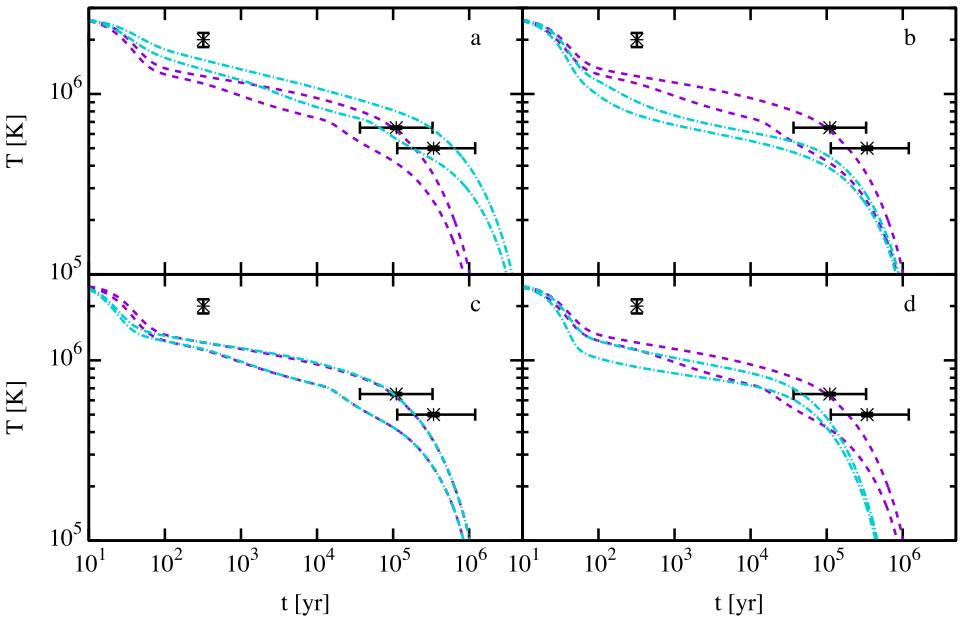

FIG. 8. Cooling tracks of neutron star models with mass $M = 1.4\ M_\odot$ for the case of a nonaccreted iron envelope ($\eta = 0$), $f_{a7} = 15$ and $\cos\beta = 0$ and 1 (upper and lower curves, respectively) and for various selections of gaps, which are specified by triples of neutron $^1S_0$, neutron $^3P_2$-$^3F_2$, and proton $^1S_0$ gaps (see Fig. 7). Each panel features the results for the triple WAP-b-T73 (dashed lines) which is used in all models shown in Figs. 2–6; the acronyms refer to Ref. [46] (WAP), model b of Ref. [47] (b), and Ref. [48] (T73), respectively. *Panel a:* Cooling tracks (dash-dotted lines) for gap triple WAP-0-T73, where 0 means vanishing neutron $^3P_2$-$^3F_2$ gap. *Panel b:* Cooling tracks for an alternate model of $^3P_2$-$^3F_2$ gap specified by the triple WAP-a-T73 (dash-dotted) lines; the acronym "a" correspond to pairing gap model a of Ref. [47]. *Panel c:* Cooling tracks for an alternate model of neutron $^1S_0$ gap specified by the triple FKC-b-T73 dash-dotted lines, where the FKC refers to Ref. [49]. *Panel d:* Cooling tracks for proton $^1S_0$ gap specified by the triple WAP-b-CCDK (dash-dotted) line, where CCDK refers to Ref. [50].

Thus, the DFSZ axion mass above the quoted values is excluded by numerical simulations of cooling neutron stars and their comparison with the observational data on Cas A.

IV. DISCUSSION AND CONCLUSIONS

In this work, we continued our study of cooling of weakly magnetized neutron stars by the emission of axions. The key strategy (see also Paper I) is to assume that the observed objects are not heavy enough to allow for nucleation of new degrees of freedom in their high-density cores. This cooling behavior could be changed significantly in cases of quark matter nucleation [51–54] or hyperonization [55–57]; for reviews see Refs. [58–61]. Even without new degrees of freedom, high densities may permit fast (or accelerated) processes involving only neutrons, protons and leptons [62,63]. For canonical mass stars with masses $M \sim 1.4\ M_\odot$ neutrino cooling is slow [41,64]. Taking the consistency of the neutrino cooling models with the data on three neutron stars with reliable fits to their blackbody emission as a reference point, we explored the modification introduced by switching on the axion emission from the stellar interior. We have included all the relevant axion emission processes which couple axions to electrons, protons and neutrons, in particular, the recently derived rates from PBF processes [9,33], as well as axion emission by electron bremsstrahlung [20,21]. The last process of electron bremsstrahlung is an insignificant source of axion emission, except when the neutron PQ charge is extremely small, so that the coupling of neutrons to axions can be neglected.

In this work, we focused on the DFSZ model which allows axion emission from the electronic component of the star. The DFSZ model has the advantage that the PQ charges of hadrons and electrons are locked via a single parameter $\cos^2\beta$. The limiting value of the axion coupling constant then spans a wide range $5 \le f_{a7} \le 15$ depending on the value of $\cos^2\beta$. This translates into a range of upper bounds on the axion mass

$$0.06 \le \max[m_a] \le 0.12\ \text{eV}, \tag{13}$$

which are consistent with those inferred for the KSVZ model.

ACKNOWLEDGMENTS

The support by the Deutsche Forschungsgemeinschaft (Grants No. SE 1836/3-2 and No. SE 1836/4-1) is gratefully acknowledged. Partial support was provided by the European COST Actions "NewCompStar" (MP1304), "PHAROS" (CA16214), and the State of Hesse LOEWE-Program in HIC for FAIR.

APPENDIX: FITS TO THE CORRELATION FUNCTIONS $F_{L/S}$

The correlation functions $F_{L/S}$ in Eq. (10) have been computed in Ref. [20]. We used the following fit formulas for these functions to implement the axion bremsstrahlung by electrons. As a function of the density these are given by simple polynomials

$$\log F_{S/L}(x,\Gamma) = a + bx^2 + cx^4 - [1 - u_{S/L}(\Gamma)], \tag{A1}$$

with $x \equiv \log\rho$ where

$$a = 0.21946, \quad b = 0.00287263, \quad c = -0.000142016, \tag{A2}$$

for $x \le x_0 = 11.4$, and

$$a = -6.47808, \quad b = 0.068645, \quad c = -0.000252677, \tag{A3}$$

for $x > x_0$. These fits were carried out for $\Gamma_0 = 10^3$ and subsequently extrapolated to other relevant values of Γ using the function

$$u_{S/L} = u_0 + u_1(\Gamma/\Gamma_0) + u_2(\Gamma/\Gamma_0)^2, \tag{A4}$$

where

$$u_0 = 0.488049, \quad u_1 = 1.25585, \quad u_2 = -0.743902, \tag{A5}$$

in the solid phase and

$$u_0 = 0.672409, \quad u_1 = 0.182774, \quad u_2 = 0.144817, \tag{A6}$$

in the liquid phase. Figure 9 shows the dependence of the correlation functions on the density on a log-log plot. The overall accuracy of the fit is below 10%, with some larger deviations $\lesssim 30\%$ in a narrow range of densities for selected values of Γ.

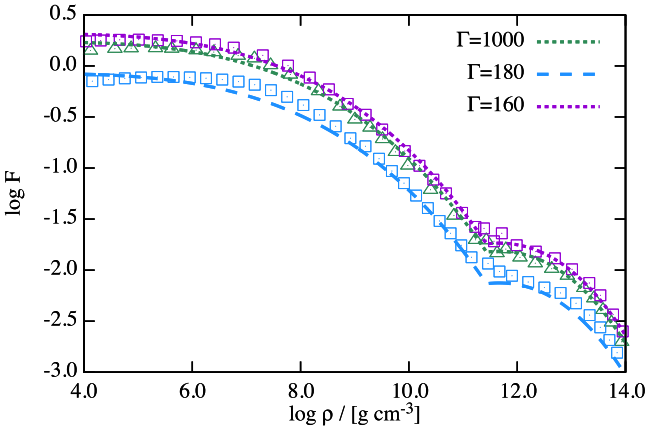

FIG. 9. Computations of Ref. [20] (points) are compared with the fits (lines) for the indicated values of the parameter Γ.

[1] F. Wilczek, Phys. Rev. Lett. **40**, 279 (1978).
[2] S. Weinberg, Phys. Rev. Lett. **40**, 223 (1978).
[3] G. 't Hooft, Phys. Rev. Lett. **37**, 8 (1976).
[4] R. D. Peccei and H. R. Quinn, Phys. Rev. Lett. **38**, 1440 (1977).
[5] R. D. Peccei, in *Axions*, Lecture Notes in Physics, edited by M. Kuster, G. Raffelt, and B. Beltrán (Springer Verlag, Berlin, 2008), Vol. 741, pp. 3–540.
[6] A. Ringwald, Phys. Dark Universe **1**, 116 (2012).
[7] M. Giannotti, I. G. Irastorza, J. Redondo, and A. Ringwald, J. Cosmol. Astropart. Phys. 05 (2016) 057.
[8] I. G. Irastorza and J. Redondo, Prog. Part. Nucl. Phys. **102**, 89 (2018).
[9] A. Sedrakian, Phys. Rev. D **93**, 065044 (2016).
[10] G. G. Raffelt, J. Redondo, and N. V. Maira, Phys. Rev. D **84**, 103008 (2011).
[11] M. Giannotti, I. G. Irastorza, J. Redondo, A. Ringwald, and K. Saikawa, J. Cosmol. Astropart. Phys. 10 (2017) 010.
[12] J. E. Kim, Phys. Rev. Lett. **43**, 103 (1979).
[13] M. Shifman, A. Vainshtein, and V. Zakharov, Nucl. Phys. **B166**, 493 (1980).
[14] M. Dine, W. Fischler, and M. Srednicki, Phys. Lett. **104B**, 199 (1981).
[15] A. R. Zhitnitsky, Yad. Fiz. **31**, 497 (1980) [Sov. J. Nucl. Phys. **31**, 260 (1980)].
[16] L. B. Leinson, J. Cosmol. Astropart. Phys. 08 (2014) 031.
[17] K. Hamaguchi, N. Nagata, K. Yanagi, and J. Zheng, Phys. Rev. D **98**, 103015 (2018).
[18] M. V. Beznogov, E. Rrapaj, D. Page, and S. Reddy, Phys. Rev. C **98**, 035802 (2018).
[19] N. Iwamoto, Phys. Rev. Lett. **53**, 1198 (1984).
[20] M. Nakagawa, Y. Kohyama, and N. Itoh, Astrophys. J. **322**, 291 (1987).
[21] M. Nakagawa, T. Adachi, Y. Kohyama, and N. Itoh, Astrophys. J. **326**, 241 (1988).
[22] H. Umeda, N. Iwamoto, S. Tsuruta, L. Qin, and K. Nomoto, in *Neutron Stars and Pulsars: Thirty Years after the Discovery*, edited by N. Shibazaki (Universal Academy Press, Tokyo,1998), p. 213.
[23] T. Altherr, E. Petitgirard, and T. del Río Gaztelurrutia, Astropart. Phys. **2**, 175 (1994).
[24] G. Raffelt and A. Weiss, Phys. Rev. D **51**, 1495 (1995).
[25] A. H. Córsico, O. G. Benvenuto, L. G. Althaus, J. Isern, and E. García-Berro, New Astron. **6**, 197 (2001).
[26] M. M. Miller Bertolami, B. E. Melendez, L. G. Althaus, and J. Isern, J. Cosmol. Astropart. Phys. 10 (2014) 069.
[27] R. P. Brinkmann and M. S. Turner, Phys. Rev. D **38**, 2338 (1988).
[28] A. Burrows, M. S. Turner, and R. P. Brinkmann, Phys. Rev. D **39**, 1020 (1989).
[29] A. Burrows, M. T. Ressell, and M. S. Turner, Phys. Rev. D **42**, 3297 (1990).
[30] H.-T. Janka, W. Keil, G. Raffelt, and D. Seckel, Phys. Rev. Lett. **76**, 2621 (1996).
[31] C. Hanhart, D. R. Phillips, and S. Reddy, Phys. Lett. B **499**, 9 (2001).
[32] T. Fischer, S. Chakraborty, M. Giannotti, A. Mirizzi, A. Payez, and A. Ringwald, Phys. Rev. D **94**, 085012 (2016).
[33] J. Keller and A. Sedrakian, Nucl. Phys. **A897**, 62 (2013).
[34] D. G. Yakovlev, A. D. Kaminker, and K. P. Levenfish, Astron. Astrophys. **343**, 650 (1999).
[35] L. B. Leinson and A. Pérez, Phys. Lett. B **638**, 114 (2006).
[36] A. Sedrakian, H. Müther, and P. Schuck, Phys. Rev. C **76**, 055805 (2007).
[37] E. E. Kolomeitsev and D. N. Voskresensky, Phys. Rev. C **77**, 065808 (2008).
[38] A. Sedrakian, Phys. Rev. C **86**, 025803 (2012).
[39] A. Harutyunyan and A. Sedrakian, Phys. Rev. C **94**, 025805 (2016).
[40] D. Viganò, N. Rea, J. A. Pons, R. Perna, D. N. Aguilera, and J. A. Miralles, Mon. Not. R. Astron. Soc. **434**, 123 (2013).
[41] D. Page, J. M. Lattimer, M. Prakash, and A. W. Steiner, Astrophys. J. **707**, 1131 (2009).
[42] E. V. Gotthelf, J. P. Halpern, and J. Alford, Astrophys. J. **765**, 58 (2013).
[43] K. G. Elshamouty, C. O. Heinke, G. R. Sivakoff, W. C. G. Ho, P. S. Shternin, D. G. Yakovlev, D. J. Patnaude, and L. David, Astrophys. J. **777**, 22 (2013).
[44] A. De Luca, P. A. Caraveo, S. Mereghetti, M. Negroni, and G. F. Bignami, Astrophys. J. **623**, 1051 (2005).
[45] B. Posselt and G. G. Pavlov, Astrophys. J. **864**, 135 (2018).
[46] J. Wambach, T. L. Ainsworth, and D. Pines, Nucl. Phys. **A555**, 128 (1993).
[47] D. Page, J. M. Lattimer, M. Prakash, and A. W. Steiner, Astrophys. J. Suppl. Ser. **155**, 623 (2004).
[48] T. Takatsuka, Prog. Theor. Phys. **50**, 1754 (1973).
[49] H.-H. Fan, E. Krotscheck, and J. W. Clark, J. Low Temp. Phys. **189**, 470 (2017).
[50] J. M. C. Chen, J. W. Clark, R. D. Davé, and V. V. Khodel, Nucl. Phys. **A555**, 59 (1993).
[51] D. Blaschke, H. Grigorian, and D. N. Voskresensky, Astron. Astrophys. **368**, 561 (2001).
[52] D. Hess and A. Sedrakian, Phys. Rev. D **84**, 063015 (2011).
[53] M. Alford, P. Jotwani, C. Kouvaris, J. Kundu, and K. Rajagopal, Phys. Rev. D **71**, 114011 (2005).
[54] A. Sedrakian, Eur. Phys. J. A **52**, 44 (2016).
[55] A. R. Raduta, A. Sedrakian, and F. Weber, Mon. Not. R. Astron. Soc. **475**, 4347 (2018).
[56] H. Grigorian, D. N. Voskresensky, and K. A. Maslov, Nucl. Phys. **A980**, 105 (2018).
[57] R. Negreiros, L. Tolos, M. Centelles, A. Ramos, and V. Dexheimer, Astrophys. J. **863**, 104 (2018).
[58] F. Weber, *Pulsars as Astrophysical Laboratories for Nuclear and Particle Physics* (Institute of Physics, Bristol, UK, 1999).
[59] A. Sedrakian, Prog. Part. Nucl. Phys. **58**, 168 (2007).
[60] D. Page, J. M. Lattimer, M. Prakash, and A. W. Steiner, in *Novel Superfluids*, International Series of Monographs on Physics, edited by K. H. Bennemann and J. B. Ketterson (Oxford University Press, Oxford, UK, 2013), p. 505.
[61] A. Sedrakian and J. W. Clark, arXiv:1802.00017.
[62] D. Blaschke, H. Grigorian, and D. N. Voskresensky, Astron. Astrophys. **424**, 979 (2004).
[63] D. Blaschke, H. Grigorian, D. N. Voskresensky, and F. Weber, Phys. Rev. C **85**, 022802 (2012).
[64] S. Beloin, S. Han, A. W. Steiner, and D. Page, Phys. Rev. C **97**, 015804 (2018).